# Appendix G:
# The Pantone "Our color Wheel" compared to the Chromaticity Diagram (2016) [1]

There is considerable interest in the conversion of Pantone identified color numbers to other numbers within the CIE and ISO Standards. Unfortunately, most of these Standards are not based on any theoretical foundation and have evolved since the late 1920's based on empirical relationships agreed to by committees. As a general rule, these Standards have all assumed that Grassman's Law of linearity in the visual realm. Unfortunately, this fundamental assumption is not appropriate and has never been confirmed. ***The visual system of all biological neural systems rely upon logarithmic summing and differencing***.

A particular goal has been to define precisely the border between colors occurring in the local language and vernacular. An example is the border between yellow and orange.

Because of the logarithmic summations used in the neural circuits of the eye and the positions of perceived yellow and orange relative to the photoreceptors of the eye, defining the transition wavelength between these two colors is particularly acute.The perceived response is particularly sensitive to stimulus intensity in the spectral region from 560 to about 580 nanometers.

This Appendix relies upon the Chromaticity Diagram (2016) developed within this work. It has previously been described as The New Chromaticity Diagram, or the New Chromaticity Diagram of Research. It is in fact a foundation document that is theoretically supportable and in turn supports a wide variety of less well founded Hering, Munsell, and various RGB and CMYK representations of the human visual spectrum. In general, it does not support any CIE Standards related to human vision; but it does provide a method for understanding how these empirical representations came about.

## G.1 The Pantone color wheel versus the Chromaticity Diagram (2016)

This section will concentrate on the development of the Pantone Color Space (known as Our Color Wheel) and the Chromaticity Diagram (2016) developed in the work, "Processes in Biological Vision" (PBV). In the development of the comparison, additional comparisons will be represented with citations to further details in PBV.

It will be asserted that there can be no precise mathematical equation(s) between these two color spaces because of the crudeness of the definition of the Pantone color space.

To quote Pantone's website,

> "In 1963, Pantone revolutionized the printing industry with the colorful PANTONE MATCHING SYSTEM®, an innovative tool allowing for the faithful selection, articulation and reproduction of consistent, accurate color anywhere in the world. The tool organizes color standards through ***a numbering system and chip format***, which have since become iconic to the Pantone brand."
>
> Elsewhere on that web page, they assert the proprietary nature of their numbering system and chip format.
>
> Pantone was acquired by X-Rite, Inc in 2007, and X-Rite was acquired by Danaher in 2012.

It is likely that Pantone originally employed several pigments well known to artists in the preparation of their color samples, such as the list on page 31 of Hope & Walch[2], an encyclopedia of color information.

### G.1.1 "Our Color Wheel" of Pantone

https://www.pantone.com/downloads/articles/pdfs/BA0646OurColorWheel.pdf provides what Pantone calls "Our color wheel." The wheel is conceptual and based on what they identify as the primary colors of red, blue and

---

[1] January 27, 2019

[2] Hope, A. & Walch, M. (1990) The Color Compendium. NY: Van Nostrand Reinhold

yellow. They then define secondary colors as green, orange and violet. Each secondary color is made of equal parts of the adjacent primaries. They then define tertiary colors as made of equal parts of the primary on one side and the secondary on the other side. The result is a wheel of only 12 discrete colors and no specific way to subdivide them. The equivalent Munsell Color Space can be subdivided into at least 120 discrete colors, hue, and an unlimited number of saturation levels. It can also accommodate a large number of lightness levels.

"The Pantone Book of Color[3]," authorized and printed by Pantone presents 1024 color swatches with fanciful names and a ink formula proprietary to Pantone. No numerical codes are associated with the color swatches in this book. The first swatch in the book, labeled "Winter White" exhibits a distinct yellow caste. The color representation on the cover does not include a central neutral (white) region.

Recently, the multiple volumes of the Pantone Book of Color include thousands of annotated color samples to support various methods of printing on packaging, textile & plastics materials.

The Pantone "Our color wheel" is neither a CMYK system used by printers in process color applications nor a RGB system as used in active sources (monitors, projection systems, etc.) It is a hybrid most closely related to the Munsell Color Space. However, it is not a direct overlay of the Munsell Color Space. They define a set of "Colors in Common" which do not conform to any other system. They do adopt the Munsell Color Space concepts of lightness (value), and saturation (hue) but then they deviate and introduce tints and shades. "A shade is the hue plus black, and a tint is the hue plus white. There are only five defined saturation steps between white and black. By combining the concepts of saturation and lightness, they obscure these independent parameters. They do not speak in terms of saturation as it is used in Munsell Color Space; zero is neutral (colorless) and the saturation can go up to (theoretical) high levels (15, 36, etc.). Simultaneously, the lightness can go from very high to very low without affecting the saturation and hue (in the first order). The Munsell Color Space illustrates second order limits on the human color space due to the signal processing inherent in the neural system.

The equivalent Munsell Color Space can be subdivided into at least 120 discrete colors, hue, and an unlimited number of saturation levels. It can also accommodate a large number of lightness levels (at least 14 on a logarithmic scale).

## G.1.2 The Chromaticity Diagram (2016)

The Chromaticity Diagram (2016) has been presented in many forms. The basic form is shown in **Figure G.1.2-1** It is developed theoretically in Part 1a of Chapter 17 beginning with Section 17.3.3 on page 238 . It is developed more fully for applications and compared with other color spaces in Part 1b of Chapter 17 beginning with a variety of definitions in Section 17.3.4 . Confirmation of the null axes at 494 and 572 nm was obtained by Wright in 1929. See page 17 of Part 1b.

The parameters, O–, P– & Q– represent the signals propagated through the neural system to the brain and represented by O = LnS - LnUV, P = LnS - LnM and Q = LnL - LnM. There is a caveat with respect to the equation related to Q that will not be introduced here. See **Section 17.3.3** in Part 1a above.

The Chromaticity Diagram (2016) is compatible with the axes of Hering Color Space, of Munsell Color Space, of RGB Color Space, and CMYK Color Space. It also provides specific wavelengths for the individual color spaces in these representations.

[3]Eiseman,L. & Herbert, L. (1990) The Pantone Book of Color. Monachie NJ: Pantone, Inc.

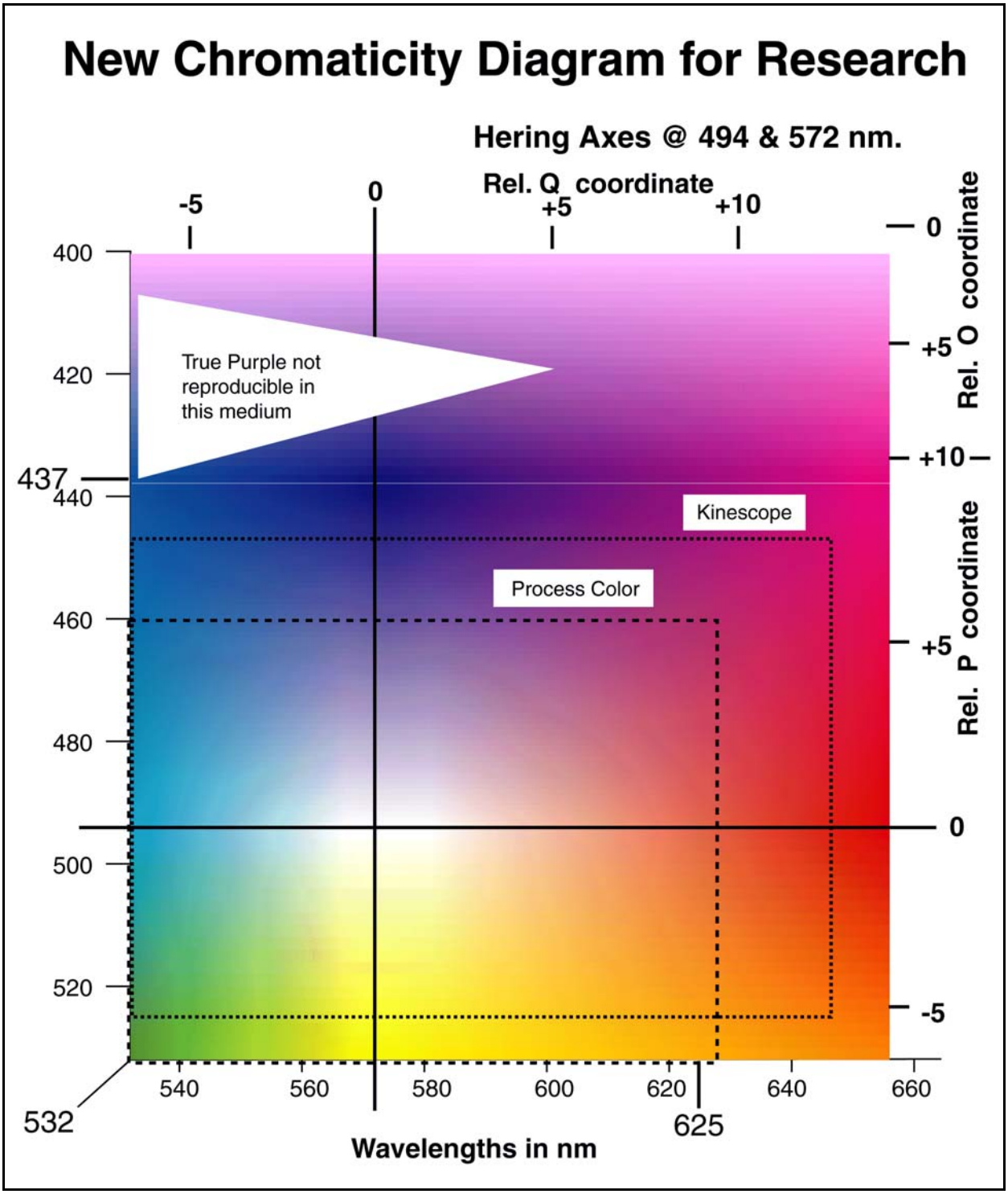


**Figure G.1.2-1 The Chromaticity Diagram (2016). The basic form is shown with the nulls at O = 0 at 395 nm, P = 0 at 494 nm, and Q = 0 at 572 nanometers representing the subtractions of the logarithms of the stimulus intensity within the neural system between the UV - S, S - M, and M - L photoreceptor channels.**

## G.1.3 The archaic CIE representations up through 1975

When initially defining the photometric performance of the human visual system, the CIE was unable to demonstrate that performance in a consistent, and mutually acceptable and collegial manner. As a result, they collected the crude data available in the 1920's and early 1930's and used it to describe a "Standard Observer," that should never be interpreted as exhibiting the average performance of the visual system of actual human observers.

The x(λ), y(λ) & z(λ) functions defined by the CIE do not even remotely resemble the actual spectral sensitivities of the chromophores of vision. Similarly defining the luminance in terms of y(λ) where this function is defined as identical to the adopted visibility function, V(λ), only complicates the problem. Finally, it is appropriate to point out the function, P(λ), used to define the power density is only appropriate if the sensory neurons of the visual modality are energy sensitive. In fact, they are fundamentally quantum counters. Using P(λ) in vision modeling discriminates against the short wavelength region of the spectrum since the photons in this area contain more energy/photon than in the long wavelength region.

### G.1.3.1 The archaic chromaticity function as an example

The CIE chromaticity diagram of 1934, modified in1951 are basically mathematical models developed in the 1920's and early 1930's when the technology available was quite limited. The various laboratories contributing to the final CIE 1934 all assumed the human neural system was based on linear summations and differences. This was a fatal error. They also used gelatin filters and low temperature light sources (around 2700 Kelvin). The gelatin filters typically had a spectral width of 20–25 nanometers wide, with very poorly defined skirts, and smeared out colors to this degree of precision. The spectral width current 5 nanometer interference filters, with very steep skirts, give totally different results. The low color temperature light sources were deficient in the blue region (although compensation was attempted in those early days). The investigators did not recognize the presence of ultra-violet photoreceptors in the human eye and theis led to major disparities among the experimenters based on the differential adaptation of the various receptors. This resulted in hilarious arguments among the principles as so well documented.

The 1961 CIE UCS (uniform color space, which included the Lab & Luv subsets) failed badly. It was based entirely on a set of piece wise linear equations that did not represent reality very well. Between 1961 and 1975, the equations representing the UCS, Lab & Luv color spaces were modified several times. The 1961 CIE UCS and its derivatives are no longer supported by the CIE

The 1976 CIE UCS dropped the Lab and Luv subsets. It remained based on a set of arbitrary piece-wise linear equations but at least they more closely matched the real world, as well as the theoretical world. See the lower right frame of figure G.1.1-2 below. The CIE 1976 UCS is relatively equiangular when overlaid on the Chromaticity Diagram (2016). However, as shown, it does not extend to the limits of the human visual space. See Section 17.3.5.4 (page 48) for more specific information.

### G.1.3.2 The archaic visibility function as an example

The so-called Photopic Visibility Function V( λ) of the CIE originally dated 1924, has been obsolete at least since the early 1950's when better instrumentation led to a new understanding of the function. Wright, one of the major participants in the development of the Visibility Function during the 1920's, provided a very interesting description of the development of the function at a symposium in 1969. Wright's words as they appear in Boynton[4], are reproduced in **Section 17.2.3.6.5**,

> "The CIE Colorimetry Committee recently in their wisdom have been looking at the old 1931 observer and have been smoothing, and interpolating, the data to obtain more consistent calculations with computers. This has also involved some extrapolation and, in smoothing, they have added some additional decimal places. When I look at the revised table of the x (bar), y(bar), z(bar) functions, I am rather surprised to say the least. You see, I know how inaccurate the actual measurements really were. (Laughter from audience) Guild did not take any observations below 400 nm and neither did I, and neither did Gibson and Tyndall on the V(λ) curve, and yet at a wavelength of 362 nm, for example, we find a value y(bar) of 0.000004929604! This, in spite of the fact that at 400 nm the value of y(bar) may be in error by a factor of 10 (Laughter)."

In 1951, Judd proposed a new photopic visibility function with significantly higher sensitivity than the 1924 standard

---

[4]Boynton, R. (1979) Human Color Vision. NY: Holt, Rinehart and Winston

in the spectral region of 400 to 450 nm. The CIE chose not to accept the Judd modification cuting the wide use of photometry based on the 1924 standard.

Wyszecki & Stiles (1982) discuss the state of the competing visibility standards available at that time (pages 392-409). The situation was so confused that their 2nd Edition of 1982 omitted a section 5.7.3 of the 1st Edition (1967) although it was called out on page 396. In the 1980 time period, the title Visibility Function was replaced by the Luminous Efficiency Function rather than the more descriptive, spectral sensitivity function of human vision.

The recent explosive growth in the application of narrow spectral band light sources based on semiconductor physics, i.e., light emitting diodes and semiconductor-based light emitting lasers, has placed new pressure on the CIE to provide theoretically-based, or at least a theory of vision compatible, visibility function.

- - - - -

**Figure G.1.3-1** compares the archaic CIE Visibility Function and recent measurements using 5 nm interference filters with virtually vertical skirts. The information in this figure is considerable and very important.

The left frame displays the CIE 1931 Photopic Luminosity fct, the CIE 1934 Scotopic Luminosity fct., and the 1958 TCI–58 Chromaticity Model of the CIE's successor organization, the Technical committee on Illumination (TCI) of the International Standards Organization (ISO). All data is presented on a relative intensity scale. The response drawn (with smoothing) through the statistical data from many observers under a variety of measurement conditions (red line) exhibits a significantly different spectral peak wavelength than the widely published CIE 1931 Photopic Luminosity fct. (previously known as the Visibility fct., V( λ); 532 nm versus the old value of 555 nm based on the Standard (unreal) Observer. This is the peak attributed to and measured for the M–channel (green) photoreceptor. It also shows peaks corresponding to the S–channel (blue) photoreceptor at 437 nm and the L–channel (red) photoreceptor at 625 nm. It also illustrates the logarithmic summation of the response of the photoreceptor, particularly in the blue-green region where the depth of the notch between them is much less than expected under the linear summation assumption.

The right frame displays data collected using 5 nm interference filters and careful attention to the differential adaptation of the eye before the start of measurements (personal communication). This author helped develop the protocol used in the experiments of Babucke and helped track down internal reflections in the instrumentation that initially distorted the data. The curve is the absolute intensity of the response of one individual in radiometric units for a fully dark adapted eye of KM. The absolute intensity threshold is remarkably constant across the human spectrum until it nears the long wavelength limit assymptote near 0.675 microns (675 milli-microns). In the short wavelength region, the threshold stimulus remained high down to at least 0.415 microns indicating the participation of the UV photoreceptor with a theoretical peak at 0.342 microns. A sharp cutoff at 0.400 microns could be expected due to the lens of the eye.

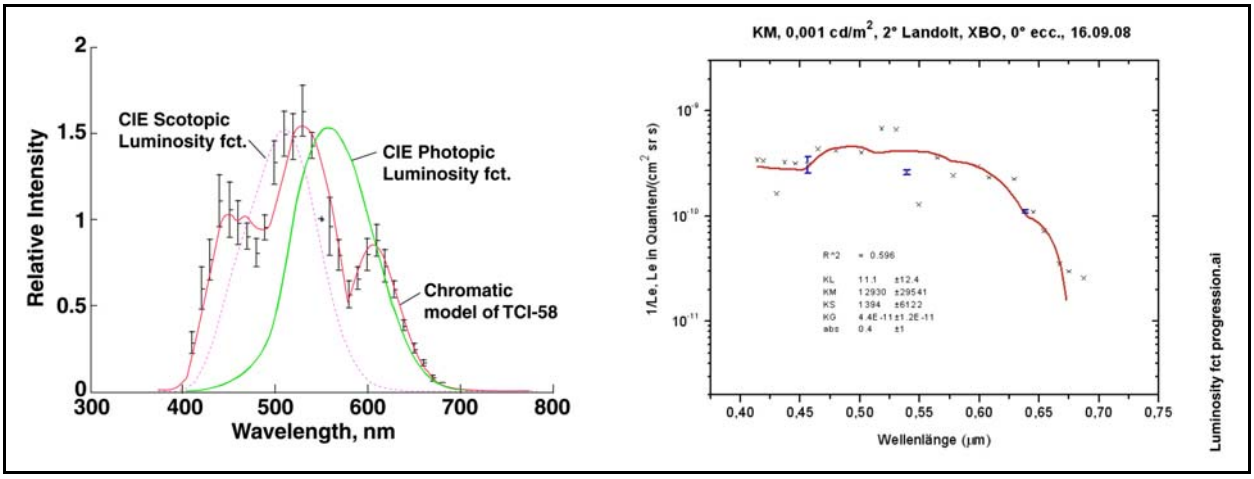


**Figure G.1.3-1 Comparison of Visibility Functions, the CIE 1931 function and a recent visibility functions using modern instrumentation. See text. Right frame from Babucke, 2008.**

In the absence of the lens (known as the aphakic condition) the response of the human retina would be expected to show a sensitivity down to about 0.320 microns as illustrated by Stark & Griswold and by Tan in **Section 17.2.3.1**.

**Figure G.1.3-2** reproduces their data.

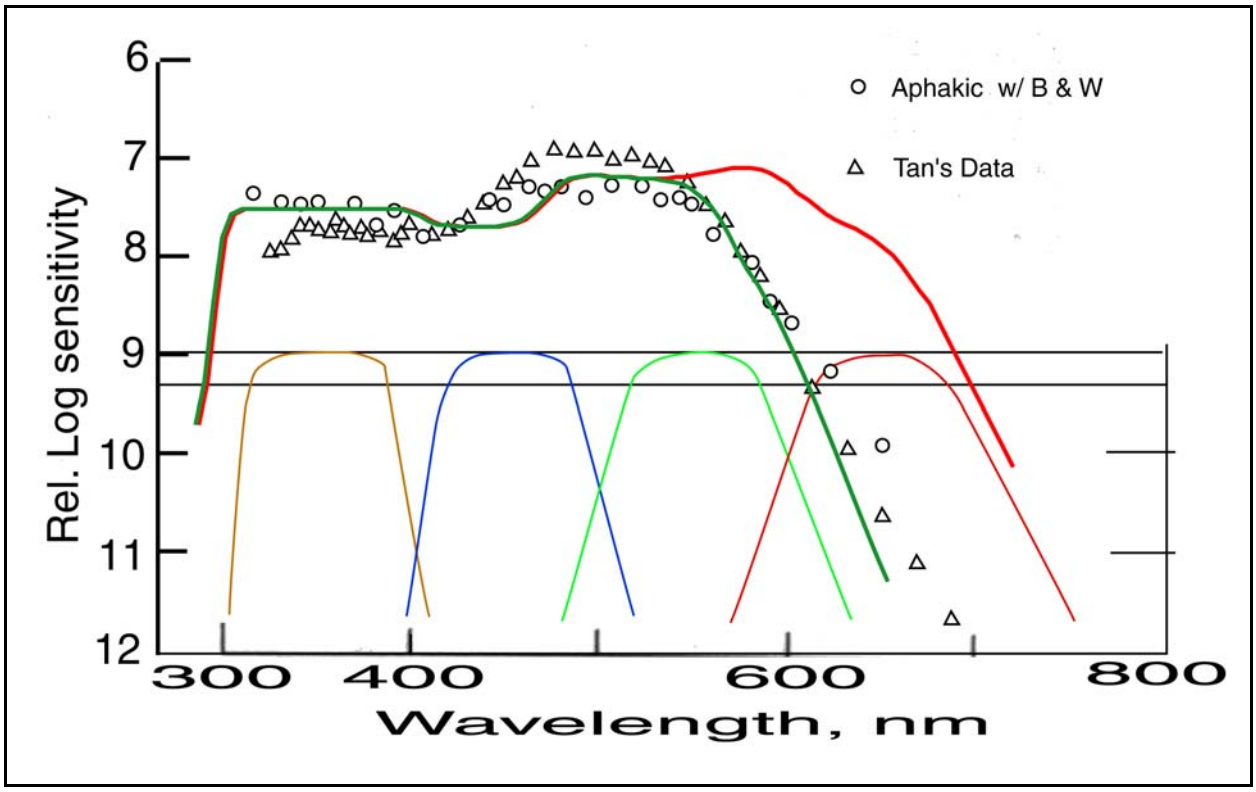


**Figure G.1.3-2 Comparison of aphakic vision and the theoretical model. The data curves were normalized with respect to each other by Griswold & Stark. The theoretical spectra are normalized with respect to each other but separately from the data. The four chromophore absorption curves are shown normalized separately as a reference. The composite theoretical curves are for a quality factor of 4.8 and are only illustrative. See text for discussion. Data points from Griswold & Stark, 1992.**

While the experimental data in the figure appears to be quite good, it must be noted that at the scale of the figure, the differences between Griswold & Stark and Tan are generally greater than 2:1. Some points differ by 3:1. The theoretical curves proposed by this work can easily be drawn within the envelope of these combined works as shown.
Thornton confirmed the theoretical spectral responses at the bottom of the figure in 1999 **(Section 5.5.10.4.3** and **Section 5.5.10.4.4**). Besides the reference absorption curves at the bottom of the figure, two composite spectral sensitivity curves are shown. The upper line (Red) is for photopic vision and the lower (Green) is for pure scotopic vision; This loss of the long wavelength performance at low stimulus levels is due the long wavelength photoreceptor responding to the square of the stimulus intensity.

The data in these sections confirm the tetrachromatic character of the human retina with spectral peaks conforming to the four photoreceptor types; Rhodonine(11) at ~625 nm, Rhodonine(9) at 532 nm, Rhodonine(7) at 437 nm and Rhodonine(5) at 342 nm. (**Section 5.5.8** through **Section 5.5.10**) There is no data in any of the representations supporting a broadband photoreceptor historically associated with a "Rod." ***The term "Rod" is archaic and never existed in a biological eye.*** It was used in ancient time, up through the 20th Century, in the absence of an adequate theoretical model and sufficiently sophisticated laboratory instrumentation.

- - - - -

Further complicating the laboratory confirmation problem is the significant difference between measurements using a filtered photometric response (with the intensity measured on a photometer) and measurements made on an equal energy basis (with intensity measured with a radiometer). The typical photometer uses a filter that is an *approximation* to the archaic CIE Visibility Function. Only measurements based on a *single* photometer or based on radiometry are reproducible.

## G.1.4 Comparison of the Pantone color wheel and the Chromaticity Diagram (2016)

**Figure G.1.4-1** compares the Pantone, "Our color wheel," to the New Chromaticity diagram with two separate overlays; a composite showing the Munsell Color Space and the capability of process color and kinescopes to reproduce the visual color range, and an overlay of the CIE UCS 1976 color space.

The frame on the lower left of this figure can be found in **Section 17.3.5.2**. The frame on the lower right of this figure can be found in **Section 17.3.5.4**.

Pantone chose to assume the primary colors of human vision are red, blue and yellow. Young (1802) was one of the first philosophers to considered the choice between red, blue and yellow primaries and red, blue and green primaries in 1802. At the time, Young vacillated between the two sets. After initially assuming the first choice, he changed his mind and ever after assumed the red, blue and green triad. As in the current Pantone case (beginning in 1963), the choice was made in the absence of any technical knowledge or viable theory. It is now clear that the photoreceptors of the eye exhibit peak sensitivities at 342, 437, 532 and between 610 & 625 nanometers (corresponding to the ultraviolet, blue, green and red spectral channels). The caveat relating to the long wavelength peak is discussed in Section 17.3.3 of Part 1a of Chapter 17. The 437, 532 and ~625 nm peaks correspond to the peaks in the individual photoreceptors of the visual spectrum measured in the laboratory. All four peaks have been measured in the laboratory on aphakic (lens-less) human eyes.

The fundamental assumption by Young, and perpetuated by the CIE since the 1930's is false. That false assumption is that the human color space is equilateral with the three primaries, red, blue and green are at the apices of such a equilateral triangle. In fact, the color channel differences represented by the O, P and Q channels of color signal information are treated as statistically independent by the brain. Mathematically, this means the channels are treated as orthogonal and can be represented by the three axes of a rectangular volume. As shown in **Section,17.3..3**, the resulting color space is a right parallelepiped with the red, blue and green signaling channels at the corners of a right triangle and not an equilateral triangle, as previously long assumed, when presented in two dimensions.

To accommodate the limited ultraviolet sensitivity of the human eye, the representation of the O– channel is rotated into the plane of the 2-dimensional Chromaticity Diagram (2016) for convenience. This means the diagram exhibits a discontinuity along the 437 nm axis. P– values larger than 10 are not shown correctly and straight lines cannot be drawn between point in the main presentation and points at wavelengths shorter than 437 nm.

Until a variant of the Chromaticity Diagram (2016) is adopted by the CIE based on a right triangle for the three corners representing the red, blue, & green primaries,, any researcher should use great caution when invoking the 1931 through 1976 Diagrams as a foundation for, as a tool in or as corroboration of his work (**Section 17.3**.3).

Pantone does not describe the wavelength of any primary color. Thus it cannot be precisely converted to any other notation.

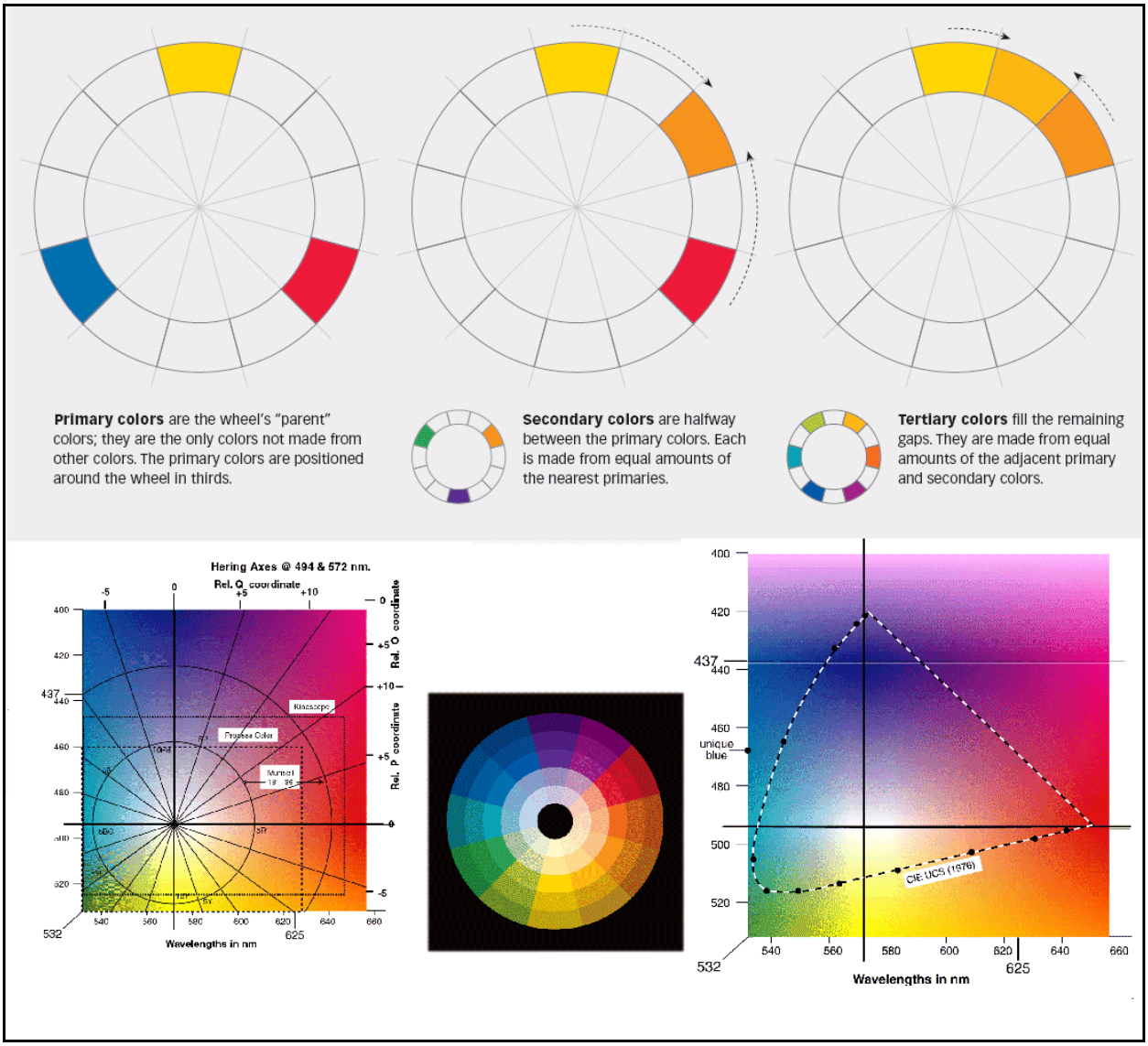


**Figure G.1.4-1 "Our color wheel" from Pantone (top) compared to the Chromaticity Diagram (2016) overlaid with the Munsell Color Space (bottom, left) and the CIE 1976 UCS (bottom, right). Also shown on the left is the capability of "process color" and kinescopes to reproduce the visual spectrum. By inverting the Pantone wheel, it can be shown (bottom, center) as an approximate overlay on the Chromaticity Diagram but it does not accommodate the cyan color at 494 nm or differentiate between red and magenta adequately. See text. Top figure from Pantone, 2019.**

The CIE chromaticity diagram of 1934, modified in1951 are basically mathematical models developed in the 1920's and early 1930's when the technology available was quite limited. The various laboratories contributing to the final CIE 1934 all assumed the human neural system was based on linear summations and differences. This was a fatal error. They also used gelatin filters and low temperature light sources (around 2700 Kelvin). The gelatin filters were typically 20 nanometers wide and smeared out colors to this degree of precision. Current 5 nanometer interference filters give totally different results. The low color temperature light sources were deficient in the blue region (although compensation was attempted in those early days). The investigators did not recognize the presence of ultra-violet photoreceptors in the human eye and theis led to major disparities among the experimenters based on the differential adaptation of the various receptors. This resulted in hilarious arguments among the principles as so

well documented.

The 1961 CIE UCS (uniform color space, which included the Lab & Luv subsets) failed badly. It was based entirely on a set of piece wise linear equations that did not represent reality very well.

Since the 1961 CIE Lab Standard, a variant of one of the subspaces, has survived, the a*,b* space. However, it remains empirically based and fails to represent the human color space adequately.

The 1976 CIE UCS dropped the Lab and Luv subsets. It remained based on a set of arbitrary piece-wise linear equations but at least they more closely matched the real world.

In the last few years, there have been many articles written describing a set of cone-fundamentals associated psycho-physically with human vision. The psychology community supports a far different set of spectral responses of the three chromophores of trichromatic vision than does the application oriented printing and display device communities. Two questions arise. First; What is the physiological relevance of the spectral color space to the chromophores of biological vision? The answer to this question would make many of the earlier papers defining the primary colors, the most vivid colors and many other designations (some of which are mentioned in Section 2.1 and Section 17.3.8 of this work) obsolete and archaic. Second; How precisely can the colors in a representation of that color space be made to agree with the absolute scale of the Chromaticity Diagram (2016)?

## G.2 The a*, b* color space

The a*, b* color space of the 1976 CIELAB appears quite similar to the McLeod-Boynton color space of 19xxx. See **Section 17.3.5.5.2**. They both introduce an alternate set of coordinates useful for low saturation colors near the neutral (white) point.

To support the above discussion, **Figure G.2.1-1** reproduces a rendition of the a*,b* color space found in Abildgaard[5]. The location of the colors varies significantly from that presented by Malacara in 2002[6]. Neither representation appears to be realistic. The Abildgaard colors seem to be too saturated for the scale locations shown. Are the scales shown the same as described by Malacara for his a*, b* color space? Malacara labeled his color locations as approximate. Figure 5.20 in the first edition of Malacara when inverted does not resemble the 2016 Diagram but Malacara did include wavelength for the termini of his axes. The wavelengths explain why his figure does not contain a neutral (white point corresponding to $L_N$). His axes when plotted on the Chromaticity Diagram (2016) is skewed far to the left (short wavelength axis). Malacara (2002) dedicated17 pages to consideration of the 1960 Luv & 1960 Lab and 1976 L*a*b* color spaces. He also provided a figure 5.10 showing the distortions in CIE x,y color space compared to that of the Munsell Color Space. His figures 5.18, 5.19 and 5.21 address the highly distorted form of the a*, b* color space. The curves in these figures all trail off toward infinity in the magenta area (as suggested by the CIE overlay on the Chromaticity Diagram 2016 in **section G.2.1** of this Appendix. Figures 5.18 & 5.19 provide scales for the a*, b* color space that may be the scales used in the Abildgaard representation.

Malacara completely rewrote the material on a*, b* Color Space in sections 6.6 to 6.8 in his 2nd Edition[7].

When inverted, the Abildgaard representation resembles the Chromaticity Diagram (2016) *but there are significant differences*. Blue is not the complement to yellow in the human (and biological) color space. Similarly, the cyan at the –a* terminus is not complementary to magenta. Cyan is complementary to a Reddish color. This should be obvious from the location of the CMY inks of the CMYK color map where the C, M & Y components are equally spaced ( 120° apart) along a circle centered on the neutral point. This figure does not accommodate the sensitivity of the human eye to wavelengths shorter than 400 nm.

---

[5] Abildgaard, M. (2013) http://michaelabildgaard.com/publications/Tryk_kontra_ISO12647_og_Pantone_v2013.xlsx

[6] Malacara, D. (2002) Color Vision and Colorimetry: Theory and Applications. Bellingham, Wa: SPIE Press

[7] Malacara, D. (2011) Color Vision and Colorimetry: Theory and Applications, 2nd Ed. Bellingham, Wa: SPIE Press

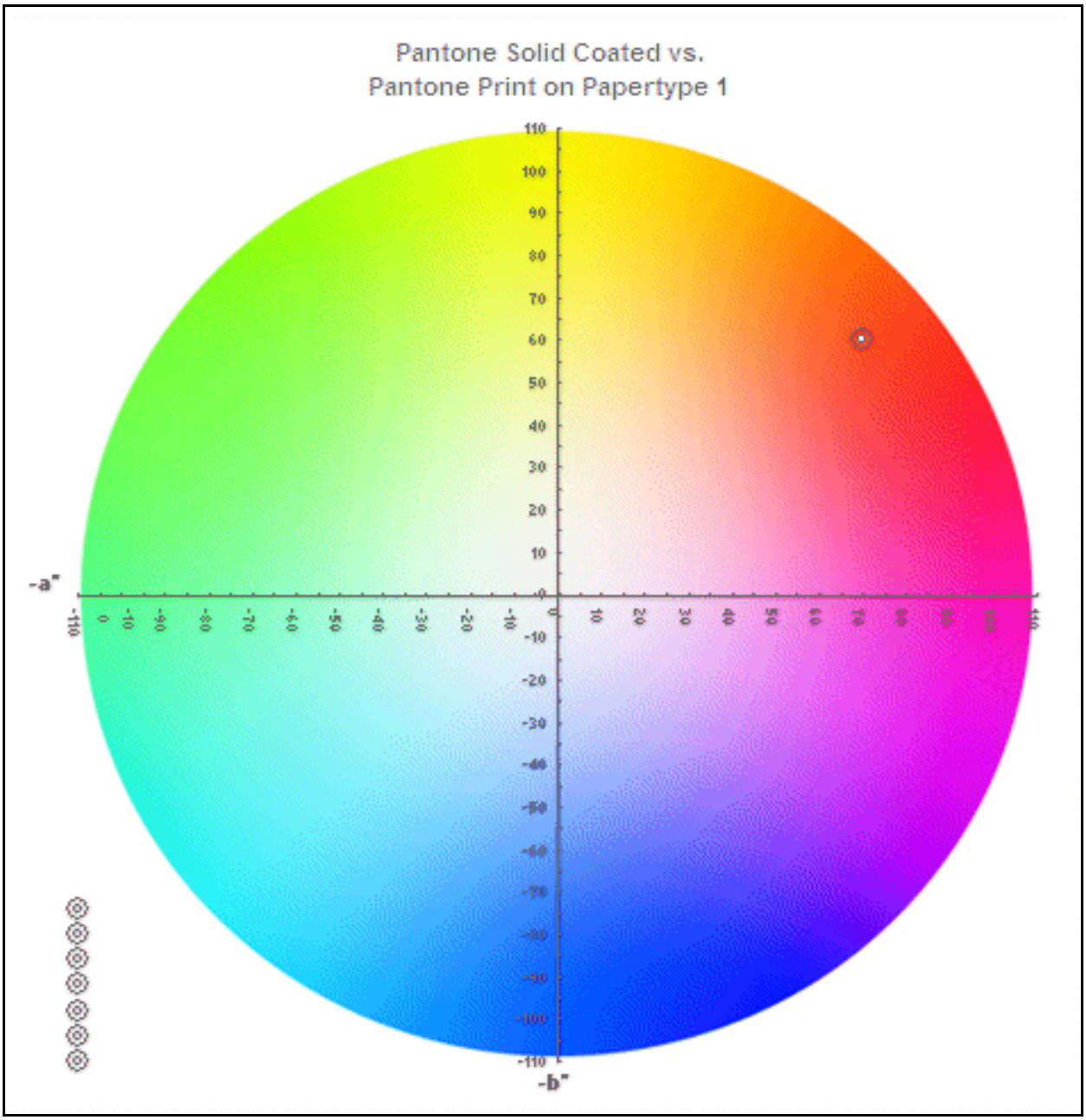


**Figure G.2.1-1 The a*, b* Color Space associated with the CIEDE 2000 Standard. The center is not defined in terms of the CIE Visibility Function of 1931. There is a typo at the termination of the –a* axis. No explanation was given for why the maximum scales are given as 110. The colors in this representation vary considerably from those of Malacara in 2002. From Michael Abildgaard, 2013.**

**Figure G.2.1-2** reproduces the Malacar figure. Without complete definition, he gave the extremes of the a* axis as at 498 nm & magenta. He gave the b* axis as extending from 475 to 574 nm. These values correspond to the defined a*, and b* axes at their intersection of the spectral locus in the CIE Chromaticity Diagram of 1931 (2° field). The unstated parameter is the color temperature used to define the white point of the CIE Chromaticity Diagram of 1931. It was most likely $D_{50}$ or ~5000 Kelvin. The colors in the figure appear to show low saturation, suggesting they are examples from near the intersection of the two axes (low saturation in the language of Munsell Color Space). Malacara did not provide scales for the a*, b* axes.

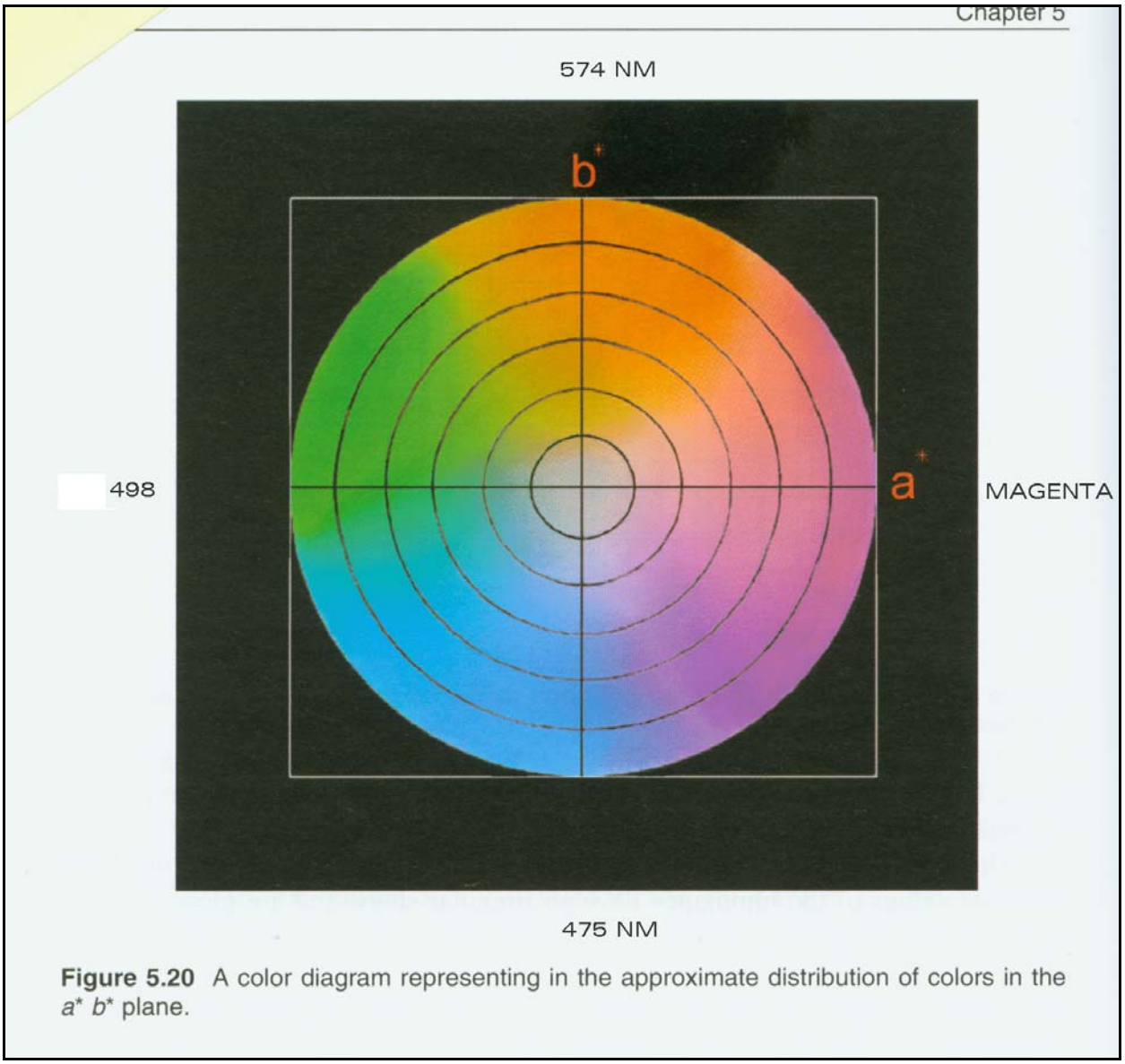


**Figure 5.20** A color diagram representing in the approximate distribution of colors in the *a* b** plane.

**Figure G.2.1-2 Alternate coloration of the a*, b* color space ala Malarca. No distinct yellow appears in the figure. The coloration in this figure appears soft. No saturated red is used. See text. From Malacara, 2002**

In his presentation at the 2004 meeting of IS&T/SID, Fairchild gives hue values of 24° for red, 90° for yellow, 162° for green and 246° for blue without further details, including the color at 0° (+a*).

There is little commonality in coloration of the a*, b* color space between abildgaard, Fairchild and Malacara. Differences of 15° are the norm. Apparently all colors were unrelated to the chromophores of human vision except the underlying framework assumes the values of the psychology community rather than the values of this work; 437, 532 & 625 nm.

## G.2.1 The character of the a*, b* color space

The character of the a*, b* Color Space has been developed in detail in **Section 17.5.3.4**. The space is deceptively distorted as shown by the ellipses overlaid on the a*, b* space in that section. The a*, b* space is far from rectilinear, and more importantly equiangular, as suggested by the a* and b* scales. Note the a*, b* axes are not perpendicular when plotted in the CIE x, y space. While the a*, b* coordinates are a linear transform of the CIE x, y space, that space is not linearly related to the human perception space. The resulting a*, b* space is also not equiangular with respect to the CIE x, y space.

Malacara has described the development of th CIE L*a*b* and L*u*v* spaces in detail[8]. Unfortunately, his drawing for the function *f*(s) is mis-drawn (fig. 5.14). He notes the color spaces were designed to apply to reflective situations and only apply over a linear range of reflectances from 0% to 100%. In practice, they only apply to a limited (but unspecified) portion of the photopic regime. **Figure G.2.1-3** shows the nonlinear axes of the CIE L*a*b* space overlaid on the CIE *x, y* Chromaticity Diagram and the isoclines of perceptual space as developed in this work.

The *alchyne* does not appear in this figure. It was originally defined as a conceptual and logical line between the most red and most blue wavelengths in the CIE 1931 x,y chromaticity diagram in the absence of any other knowledge.

Fairchild also addressed the updates in the definition of the a*, b* space in 2004[9]. Unfortunately, the paper and subsequently published book suffers in at least two respects; 1) He uses the psychology communities assertions that the spectral peaks in the visual spectrum occur at approximately 430, 550 and 580 nm., 2) he made several assertions associated with the human visual system that are not in agreement with reality. His material is reviewed in **Section 17.3.5.4.3**.

The actual peak sensitivity of the three chromophores of biological vision (ignoring the UV chromophore) are shown in as Figure 4.4 in Malacara (2011). Avoiding the *negative value* in the *r*-bar(λ) at 520 nm, which is impossible, is imperative. It occurs due to the false assumption that the linear assumption of CIE theory embraced in the equation,

$r(\lambda) + g(\lambda) + b(\lambda) = 1.00$ False!

and the no longer viable assumption that the human visibility function even remotely resembles the V(λ) of the CIE Standard Observer apply. The actual biological visual modality employs

$\mathrm{Ln}(r(\lambda)) + \mathrm{Ln}(g(\lambda)) + \mathrm{Ln}(b(\lambda)) = K$ True

and the actual visibility function of the general population of human eyes is shown in **Section 17.3.7.6**. The actual use of the logarithmic equation, and the real visibility function of the human observer, can be demonstrated in the laboratory (See recent data of Babucke, personal communication, in **Section**

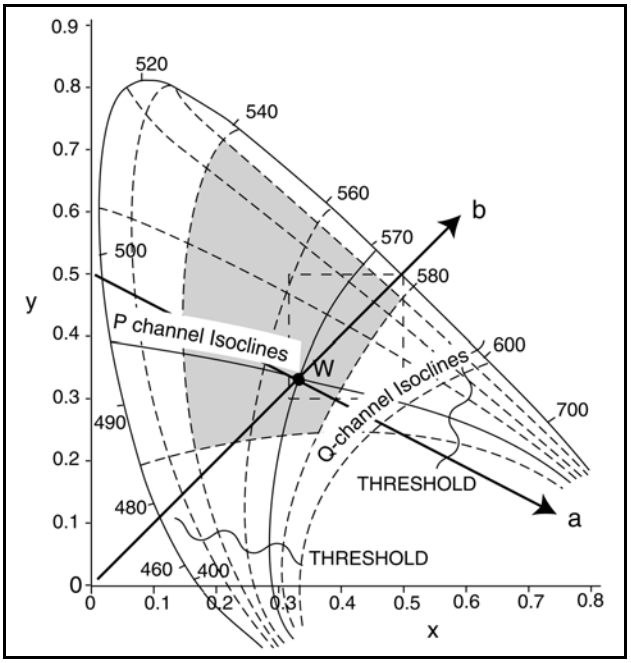


**Figure G.2.1-3 The a*b* axes of CIELAB overlaid on the CIE x,y Chromaticity Diagram. The a*b* axes are not orthogonal in *x,y* object space. Neither do they follow the isoclines reflecting perceptual space. The nonlinear formula for a* and b* stretch the above figure along these axes when plotted using the linear coordinates of L*a*b* color space. Axes from Malacara, 2002.**

[8]Malacara, D. (2002) Color Vision and Colorimetry: Theory and Applications. Bellingham, Wa: SPIE Press

[9]Fairchild, M. (2004) Color Appearance Models: CIECAM02 and Beyond. RIT Munsell Color Science Laboratory www.cis.rit.edu/mcsl Now published in Fairchild, M.D. (2005) Color appearance models, 2nd ed.). Hoboken, NJ: Wiley.

**17.3.7.6**). It avoids the need for the non-conformal transformation that Malacara (2011) reviewed on pages 75 to 81.

On page 75 discussing bipartite color matching, Malacara asserts the well known failure of the linear assumption in CIE theory, "For some wavelengths of the monochromatic reference, after decreasing the luminance of the red beam in the matched zone to zero, the color may still look too red. The only solution in order to achieve a perfect match is to add red to the reference zone, instead of taking it from the sample, *which is impossible* [emphasis added]." He also notes that a projective transformation to solve this difficulty has been suggested at least since 1915. On page 76, he evaluates the terms of such a projective transformation in matrix form under the arbitrary assumption that V(λ) actually represents the visibility function of a human. On page 77, he notes, "The fourth condition (in solving the matrix) is that the *y*-bar axis must be tangent to the curve, so that no value of *x*-bar(λ) is negative." He then gives an equation for *x*-bar(λ) and notes, "and this function has a minimum that can be pushed down or pulled up by changing the value of the coefficient $a_{11}$." He illustrates this solution in figure 5.1 of the 2011 edition. The figure shows the log wavelength color matching function with a secondary peak near 450 nm. No such secondary peak has never been associated with any long wavelength chromophore! ***This use of a non-conformal transformation and ficticious V(λ) to achieve the desired result is very clever means of solving a problem that exists in the protocol used to obtain the raw data but lacks any physiological basis in the visual modality***.

## G.2.2 The a*, b* color space overlaid on the Chromaticity Diagram (2016)

It is difficult to overlay an imprecisely defined and empirical color space, such as the a*, b* space on the theoretically supported, and both rectilinear and equiangular, color space of the Chromaticity Diagram (2016). **Figure G.2.2-1** shows a first attempt to (freehand) overlay the a*, b* axes on the Diagram. As noted in the caption, the axes were drawn based on Malacara's data in his 2002 book. The axes shown correlate well with his figures 5.18, 5.19 & 5.21. The axis disappearing in the magenta region is elongated in these figures.

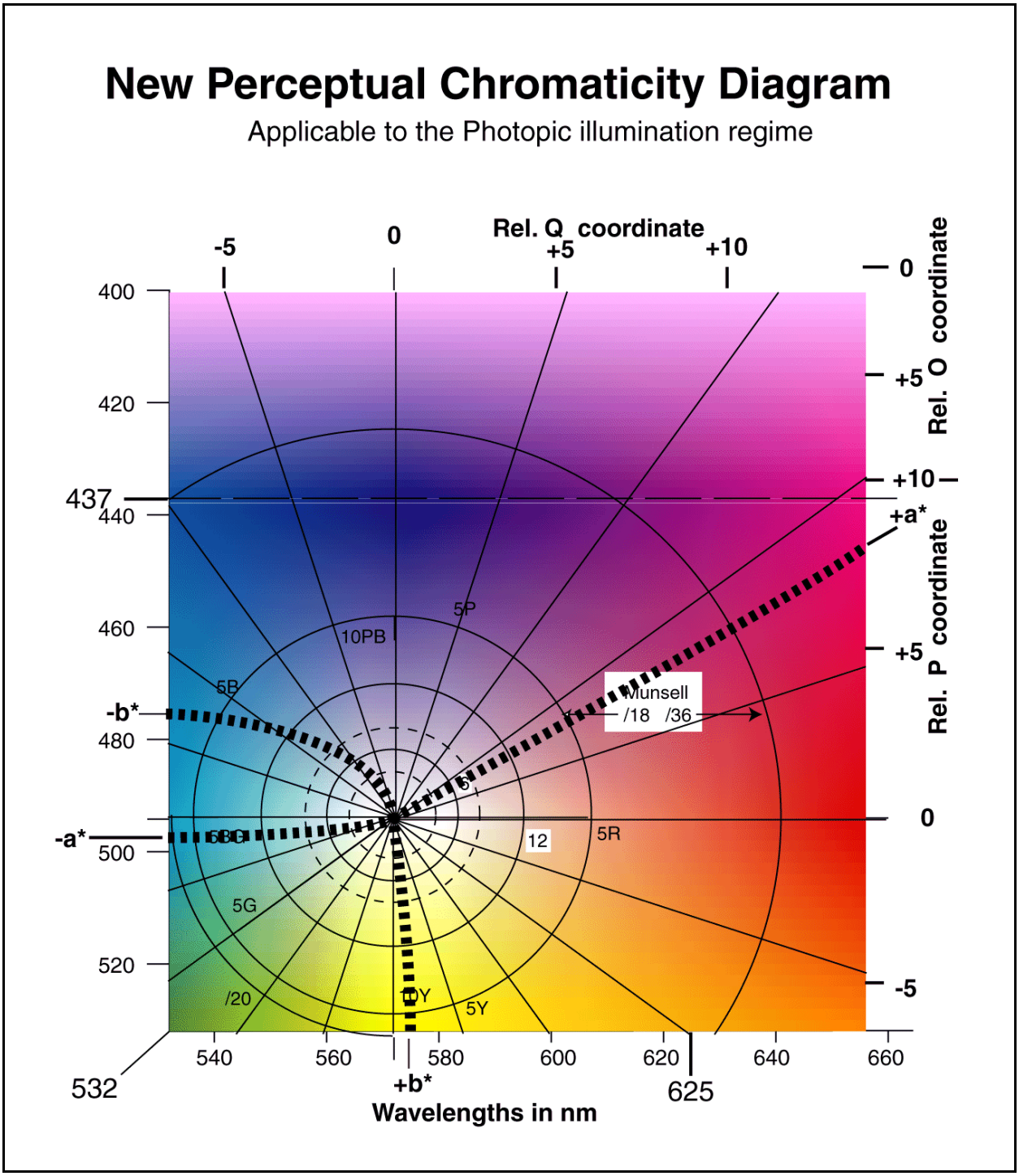


**Figure G.2.2-1 a*, b* axes overlaid on the Chromaticity Diagram (2016). The a*, b* axes (heavy dashed lines) are drawn freehand based on the data of Malacara (2002). Malacara's axes were not perpendicular at their junction when drawn on the CIE 1931 Chromaticity Diagram. The axes are warped significantly when displayed on an orthogonal (both rectilinear and equiangular) color space.**

## G.2.3 The a*, b* color space overlay in finer detail for small chroma (saturation)

The great curvature of the a*, b* axes when plotted on the complete Chromaticity Diagram (2016) suggests a study in greater detail at low chroma values surrounding the neutral (white) point might be fruitful. Malacara offers such a a separate comparison of the a*, b* Color Space with the Munsell Color Space as an overlay. **Figure G.2.3-1** reproduces his figure, indicating a clear relationship between the a*, b* colors and the Chromaticity Diagram (2016) and the limits of the a* ,b* color space. What is not provided in this figure is the accompanying statistics. Was this data gathered from only one individual or is a summary from multiple test subjects? Are error bars available if the data was gathered from multiple test subjects, or, for multiple matches performed by one individual. A critical factor is what colors were assigned to the a*, b* space when attempting to match the color swatches of the Munsell Color Space?

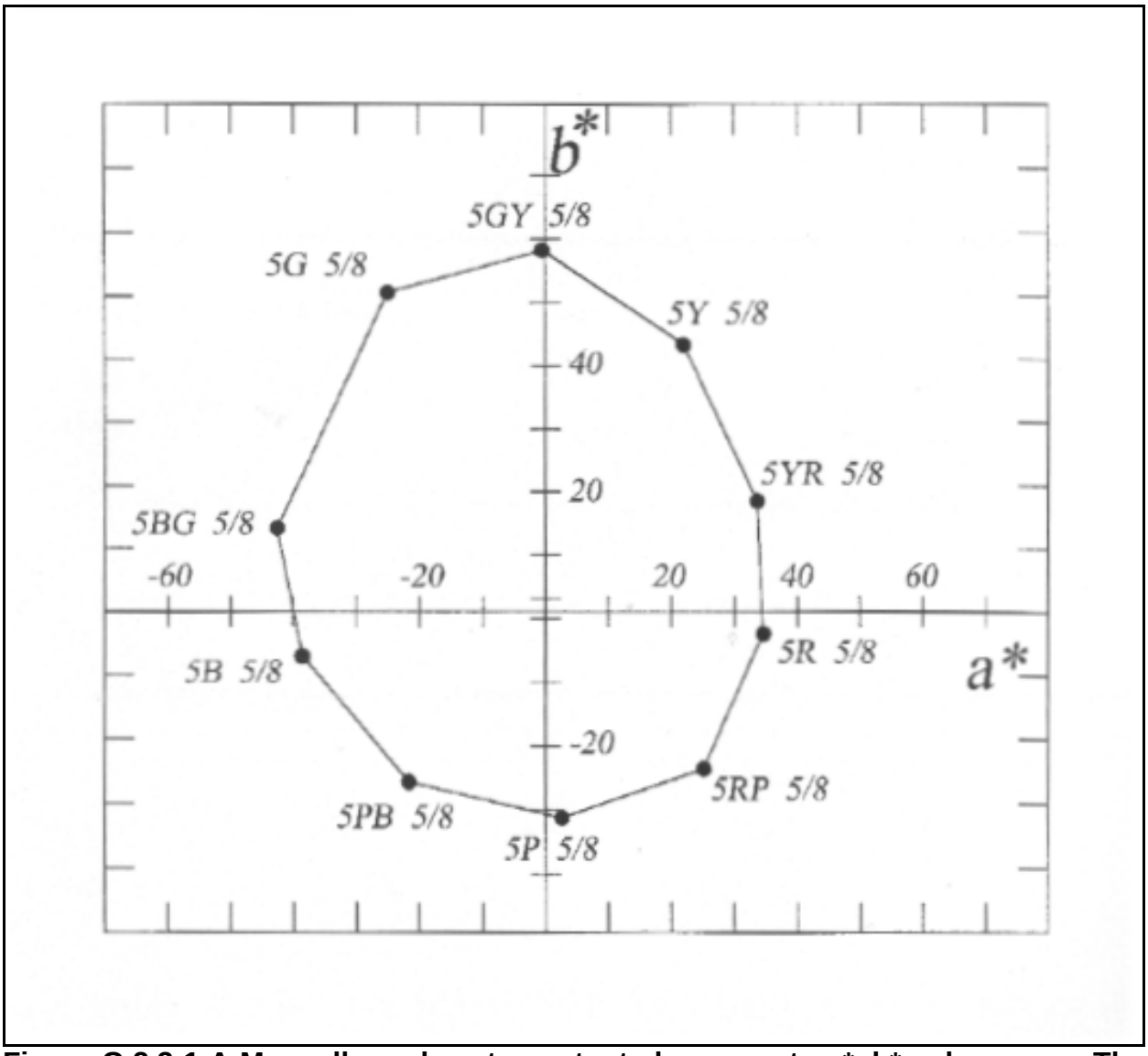


**Figure G.2.3-1 A Munsell overlay at constant chroma onto a*, b* color space. The oblong nature of the ovelay is due to the non-orthogonal character of the a*, b* color space. See Text. From Malacara, 2002.**

When the Malacara a*, b* color space is overlaid on the Chromaticity Diagram (2016) along with the Munsell color spaces in **Figure G.2.3-2**, the relationships between the three is easily seen. The a*, b* axes are rotated 16 ± 1 degrees from the rectilinear spectral axes of the Chromaticity Diagram (2016). The +b axis points toward the bottom of the figure, parallel to the 5GY radial of Munsell. The elipsoid from Malacara was scaled to determine the best fit of individual points to the Munsell radial label of the data points. The data from Malacara for chroma /8 appears to be a better match to chroma /4 based on the scales from Munsell in the combined graphs. This difference may deserve additional analysis. The distortion in the 10G to 5Y region can be associated with the non-orthogonality of the a*, b* axes far from their intersection as shown in **Figure G.2.2-1**. It is likely that the ellipsoid of Malacara will become even more ellisoidal for values of chroma (saturation) higher than his /8!

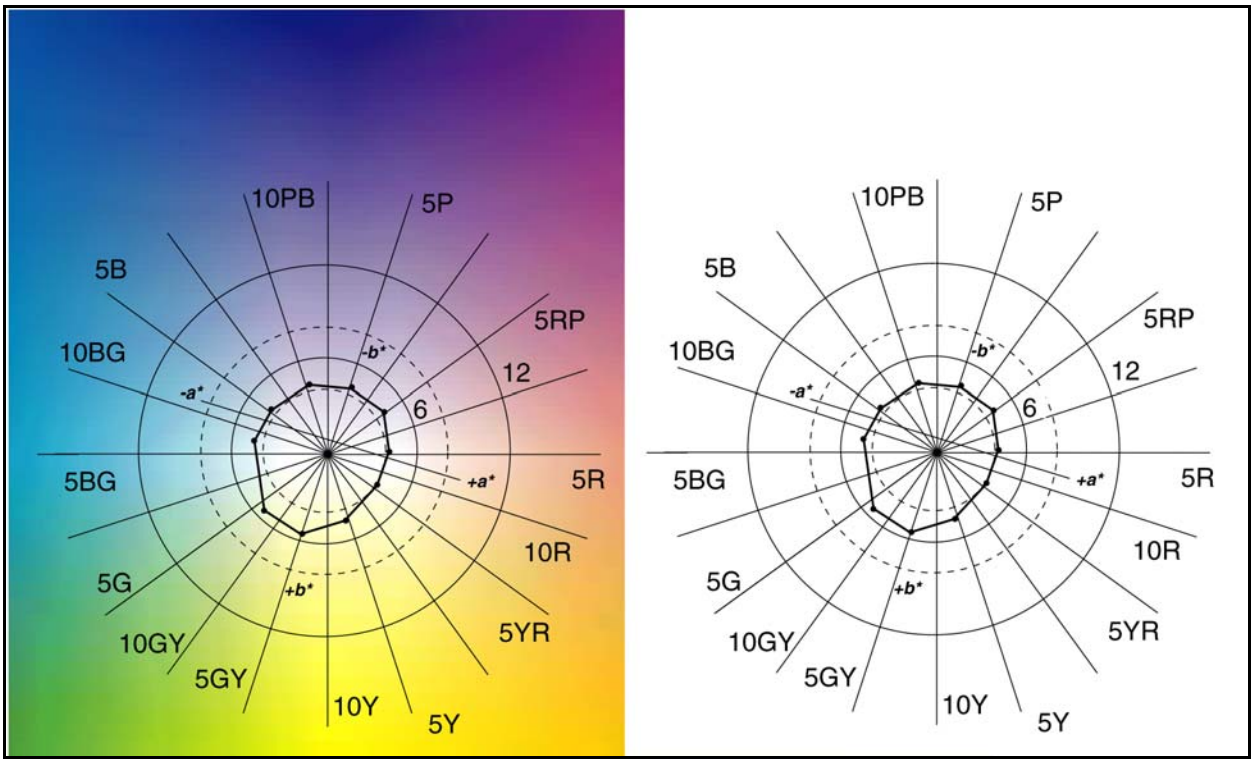


**Figure G.2.3-2 The center of the Chromaticity Diagram (2016) with a*, b* overlay. Left in color; right in black & white. The distortion of the a*, b* color space is apparent within chroma = /6 of the Munsell space. The data points on the ellipsoid of Malacara relate to his chroma value of 5; they seem to relate to chroma 4 (dashed line under ellipsoid) in this representation. The axes of the a*, b* color space are rotated 16 degrees from the axes of the Chromaticity Diagram (2016) in this best fit overlay using the data points as a reference. The distortion in the direction of the +b* axis is apparent. The colors on the right representations are the same as used throught this work. See text. Overlay from Malacara, 2011.**

### G.2.3.1 Corrections required to the CIELAB formulas

There are three problems with the current equations defining the CIE 1976 L*A*B* color space. They will be addressed in order of importance. First, it is inherently not rectilinear and equiangular for even small values of chroma. Second, its current +b* to -b* axis is not parallel to the natural spectral locus. These two conditions make it awkward to consider translations between the L*a*b* color space and any other color space with precision. Third,

the equation for Lightness, L, needs to recognize the term, $L^{1/3}$, frequently used in that defining equation should be rewritten as Ln(L) with a subsequent interpretation of that equation (with out the piece-wise linear formalism).

As shown in **Section G.2.1** and **Section G.2.2**, the axes are not orthogonal, even though this is usually ignored in standalone applications of the a*, b* color space (where the axes are drawn as orthogonal). At higher chroma (saturation), the axes are not even straight with respect to the Chromaticity Diagram (2016) or Munsell Color Space.

The rectilinearity at small chroma values, possibly less than /8, adequate rectilinear performance can be achieved by redefining the equations of the CIE 1976 L*a*b*

- - -

The following subsections will discuss the recommended modifications to the equations defining the CIE 1976 L*a*b* space to make them compatible with other color spaces and improve their internal integrity (not plotting inherently skewed axes using a rectilinear grid). These recommended modifications should be considered in one overall modification, but they are addressed here individually for pedagogical purposes.

The numerical values recommended in the following subsections should be considered preliminary until more substantive comparisons are made in the laboratory.

## G.2.3.1.1 Recommendation to correct rectilinearity at low chrominance values

Looking at the graph in **Section G.2.1**, it appears the original investigator chose the b* axis of the CIE 1976 L*a*b* coordinates to pass through x = y = 0.00 and a null (white) point of on defined color temperature, on the CIE 1931 Chromaticity Diagram. He then chose the a* axis to pass through the same null point and the spectral locus value of 498 nm.

The ideal would be to use a defined null point based on a specified color temperature of $D_{50}$, 5000 Kelvin, or higher if work in the short wavelength regions is important.

The ideal would be to make the coordinates parallel to the P and Q axes of the Chromaticity Diagram (2016) and the Munsell Color Space.

Rectilinearity can be most easily achieved by removing the x = y = 0 criteria and using the null point and the spectral value of 568 nm to establish the b* axis. This would provide a rectilinear a*, b* space with respect to x, y space, and with the b* axis nearly parallel to the Q- isoclines of the Chromaticity Diagram (2016). However, the axes would not be at right angles in the Chromaticity Diagram (2016).

To achieve rectilinearity in the color space of both Munsell Color Space and the Chromaticity Diagram (2016), the b* axis and the a* axis must be parallel to the P- and Q-isoclines. This would require the b* axis to pass through the null point and 568 nm and the a* axis to pass through the null point and the spectral locus at 494 nm. This would result in a revised set of a*, b* axes as shown as an overlay in **Figure G.2.3-3**. The result would be an a*,b* Color Space that would share axes when superimposed on either the Munsell Color Space or the Chromaticity Diagram (2016) at chroma (saturation) values below /8. Of course, unless the b* axis was reversed in the figure shown, the +b* axis would point downward when so overlaid.

*A fuller recommendation would be to reverse the b* axis direction.* This is the situation shown in the figure. This change also results in the a*, b* coordinates being compatible with the coordinate directions in most related color space presentations. It places yellow at the bottom of the representation.

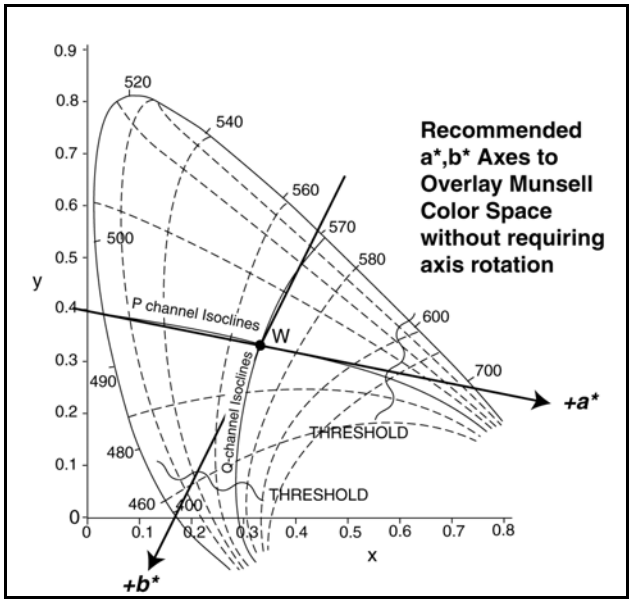


**Figure G.2.3-3 Recommended modification to the CIELAB color space to overlay the Munsell and Chromaticity Diagram (2016) Color Space and thereby sharing the same axes at low saturation values.**

## G.3 The definition of the pigments and lights optimally describing the human color space

With the Chromaticity Diagram (2016) available, it becomes possible to more specifically define the appropriate pigments for subtractive "process color printing" and the lights of additive color display as used in most monitors, etc.

> According to Malacara (2011, page 140), among the colorants, dyes and pigments can be distinguished. "Technically speaking, dyes are soluble in the host material, typically water, while pigments are not. Another difference is that dyes do not scatter light, and they look transparent. On the other hand, pigments scatter light and thus, are opaque. Still another difference is that dyes are absorbed by the colored substrate, while pigments require a binder to stick to the surface...Definitions given in dictionaries or used in some industries do not necessarily coincide with these ideas."

### G.3.1 The character of the Chromaticity Diagram (2016)

In the new physiology-based Chromaticity Diagram (2016, the principle colors are not equally spaced about a circle. As shown in **Figure G.3.1-1** reproduced from **Section 17.3.8** and **Section 17.3.9**, where the Munsell color Space is overlaid on the Chromaticity Diagram (2016). The peak wavelength of the actual chromophores of the sensory receptors are shown at 437 nm (spectral blue), at 532 nm (spectral green) and at 625 nm (spectral red). Intuitively, maximally effective stimuli would have their energy centered on these wavelengths. This would be true for both active sources as well as the subtractive situation known as process color printing. The maximally effective stimuli presented to the biological eye will consist of energy concentrated at one or more of these wavelengths.

Using the Munsell Color space, the maximally effective stimuli will correspond to stimuli corresponding to high saturation values along the 10B (blue), 2.5GY (green) & 5YR (red) radials. As shown, the maximally effective stimuli will have saturation values between 20 and 34. Narrow spectral band lights with spectral centroids falling along these radials will be maximally effective at stimulating the chromophores of the visual modality. The angle between the maximally effective blue and green radials is 92.5°. The angle between the maximally effective green and red radials is also 92.5°. The angle between the maximally effective red and blue and red radials is either 185° or 175° depending on which direction you prefer to travel circumferentially around the Munssell Color Space.

In the case of process color, it is pigments with the centroid of their spectral wavelength at the complement of these wavelengths that will be most effective. However, in this case, the spectral widths of their absorption spectrum should be sufficiently wide to block light from reaching the other two primaries. This makes the location of the centroid of the notch in of the absorption spectrum less important than in the case of stimulating lights. Limiting the

discussion to the nominal process color region indicated by the dashed box, The nominal centroid of the pigment blocking all but the green light will be along the 2.5RP radial. The notch in the absorption spectrum of this pigment will be located at 2.5G. The centroid of the absorption spectrum of the commonly used magenta at this location can also be specified as the intersection of the two spectral values, 460 and 610 nm or 460,610. Similarly, the subtractive pigment blocking all but the blue light reflected from the paper would be optimally centered at 10YR with a notch in the absorption at 10B Similarly, the subtractive pigment blocking all but the red light reflected from the paper would be optimally centered at 10B with a notch centered on 10YR.

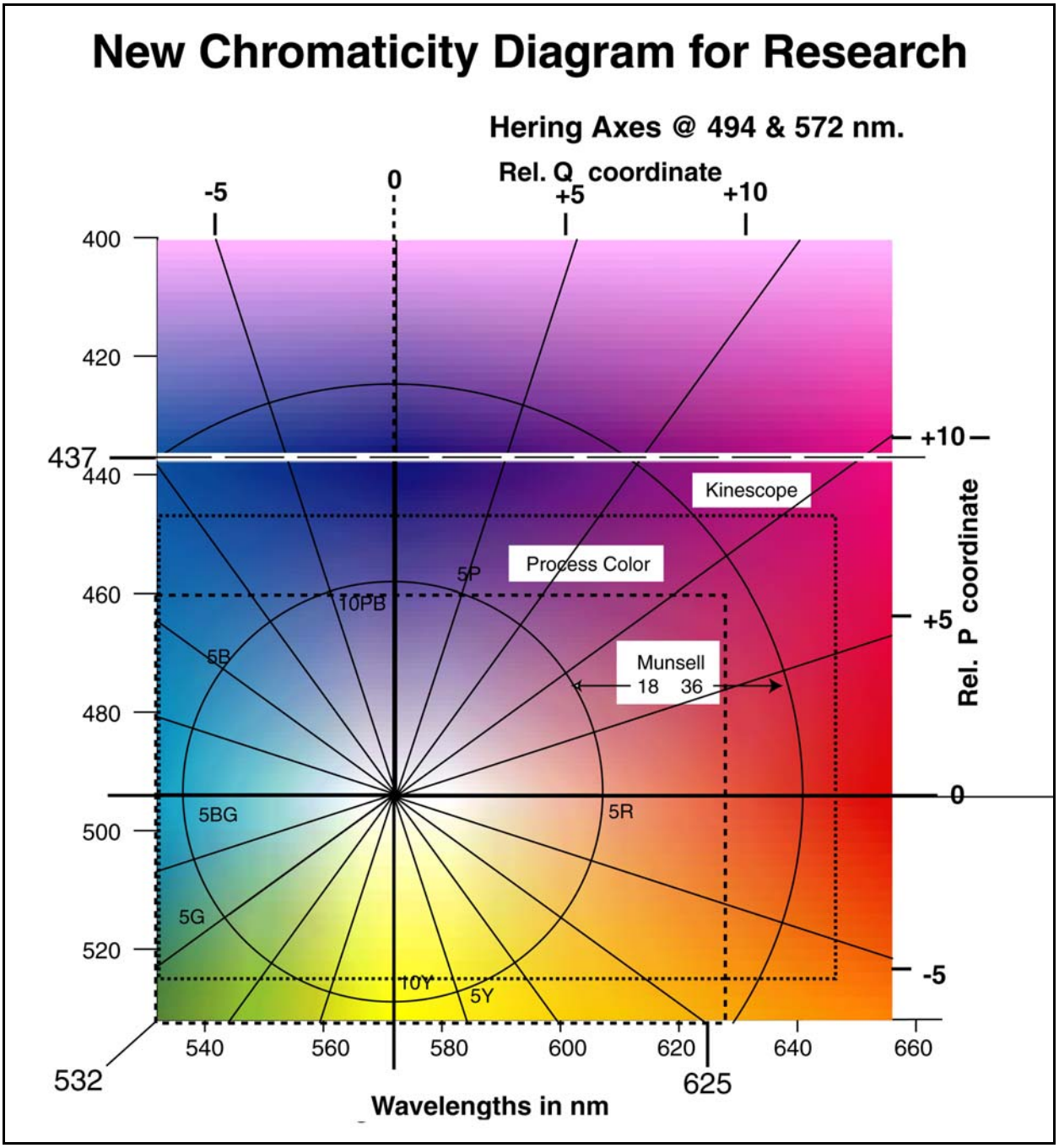


**Figure G.3.1-1 Definition of the primary colors and their complement in human color space. Both the optimum RGB and CMYK color sets are shown. See text.**

## G.3.2 The spectra of ideal process color filters

By unraveling the spectral locus from 400 nm to 655 nm, into a ribbon graph, the consequences of the choices for the pigments used in the process color are more obviously envisioned. **Figure G.3.2-1** presents the ideal filters of process printing according to Malacara (2011).

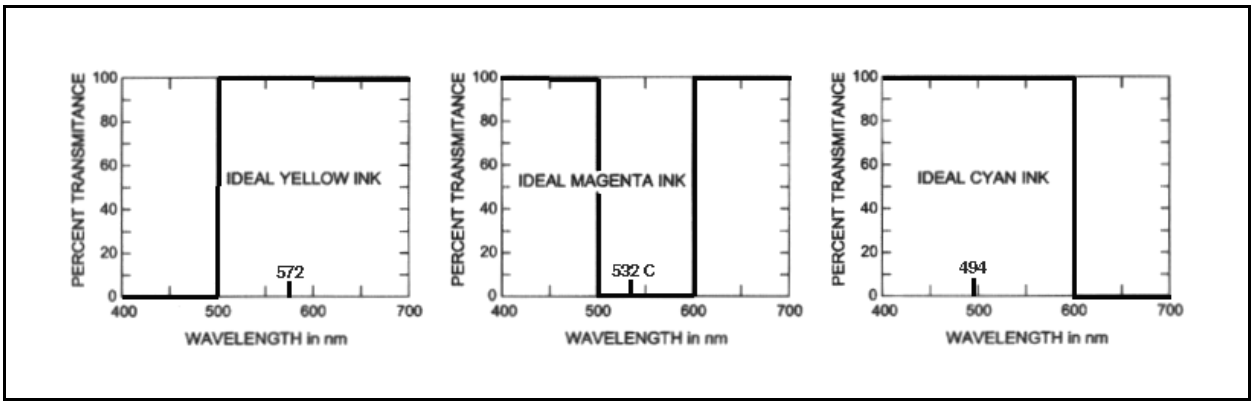


**Figure G.3.2-1 The ideal choice for the filters used in process color printing. The values shown, 494 & 572 nm have been added. They are the conventional center values for yellow and cyan (azure). The value of 532 C is the complimentary address for the magenta ink. From Malacara, 2011.**

If the blocking filters do not extend across the entire visible spectrum, some leakage may occur resulting in a "muddy looking" final image on a substrate (most likely coated paper or cardboard). Because of the likelihood of some leakage with available pigments, it is common to use a fourth black pigment to overlay the previous application of the three blocking pigments, resulting in the what is traditionally called the Cyan-Magenta-Yellow-Black (CMYK) color printing process. Ideally, the black layer has a very low transmission across the entire spectral band.

As noted above, the traditional cyan-magenta and yellow blocking filters are nearly ideal based on the Young (1802) concept of color vision based on an equilateral triangle. However, in fact, the ideal filters shown need not appear to be one of these colors to the naked human eye. The ideal filters would all appear opaque except for the region of high transmittance.

## G.3.3 Review of the coloration of Abildgaard's version of the CIEDE 2000

**Figure G.3.3-1** repeats the earlier figure from Abildgaard related to the CIEDE 2000 Standard with selected Munsell radials added to evaluate the coloration shown. The coloration agrees with the Munsell axes and the P =0 radial labeled 5BG that should be "colorless" or neutral. 5BG is sometimes described as the narrow band color, azure, and is the potential center of the broadband cyan of process color printing. Similarly, the 10Y radial corresponds to Q = 0 that represents a maximum perceived Yellow in Munsell Color Space. The Munsell coordinates do suggest the area shown in blue should be rotated into the lower left quadrant and the area shown in Magenta (or purple or violet) should be extended to include the 10PB radial. Purple and/or violet would then be found in the region of h*300 to h*310 in a*, b* space or 10B to 5PB in Munsell Color Space.

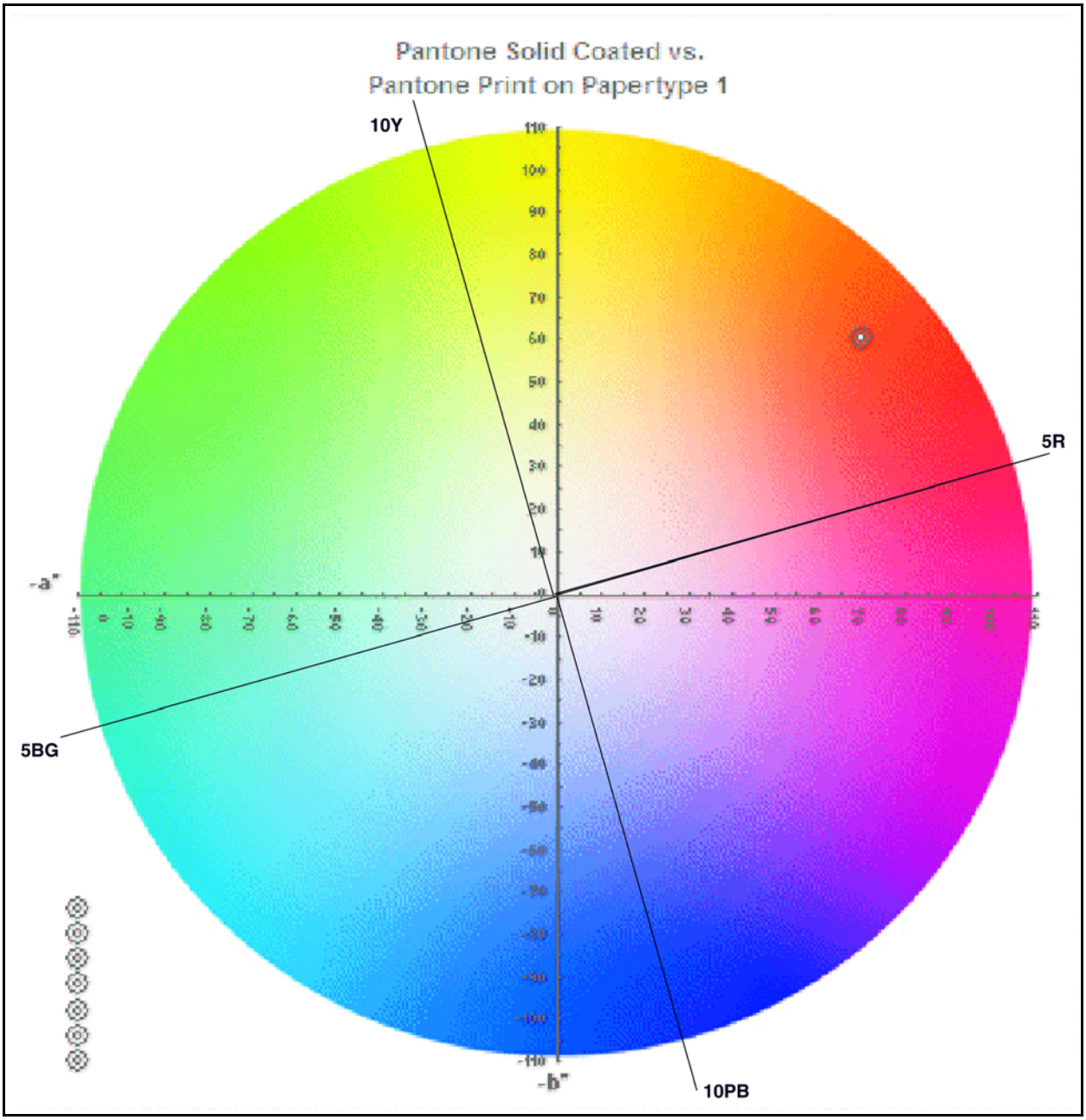


**Figure G.3.3-1 The a*, b* Color Space associated with the CIEDE 2000 Standard with the axes of Munsell Color Space overlaid. The coloration agrees quite well with the Munsell coordinates except in the lower right. The magenta should extend to beyond 10PB with blue pushed around the circle into the lower left quadrant. See text. The colored a*, b* space from Michael Abildgaard, 2013.**

## G.4 Defining Pantone color swatches within Color Spaces of the scientific community

There is a desire within the graphics community to relate the color swatches of the various Pantone color systems to a theoretical framework. It appears this can be done. The major problem is determining the actual chromatic

coordinates of the Pantone color system of interest. Pantone appears to treat their numbering systems as proprietary. Thus, the challenge is to obtain reproducible spectral values for the Pantone swatches of interest.

One method is to compare a given set of Pantone swatches of interest to the equivalent Munsell Color System swatches that are directly relatable to the Chromaticity Diagram (2016). This method leads to an absolute spectral address for each Pantone swatch regardless of the proprietary character of the Pantone numbering system. While laborious, this method would result in a mapping of the Pantone numbering system onto the Diagram. This mapping may result in a single equation describing the absolute spectral addresses of the Pantone swatches versus their Pantone number. Alternately, it may demonstrate that a series of piece-wise equations are required to describe the absolute spectral addresses of the given Pantone set of swatches.

An alternate method is to collect data related to the Pantone swatches available in the literature and compare that data with the Chromaticity Diagram (2016). An example of this approach has been provided to this investigator by Abildgaard [xxx ] as shown in **Figure G.4.1-1**

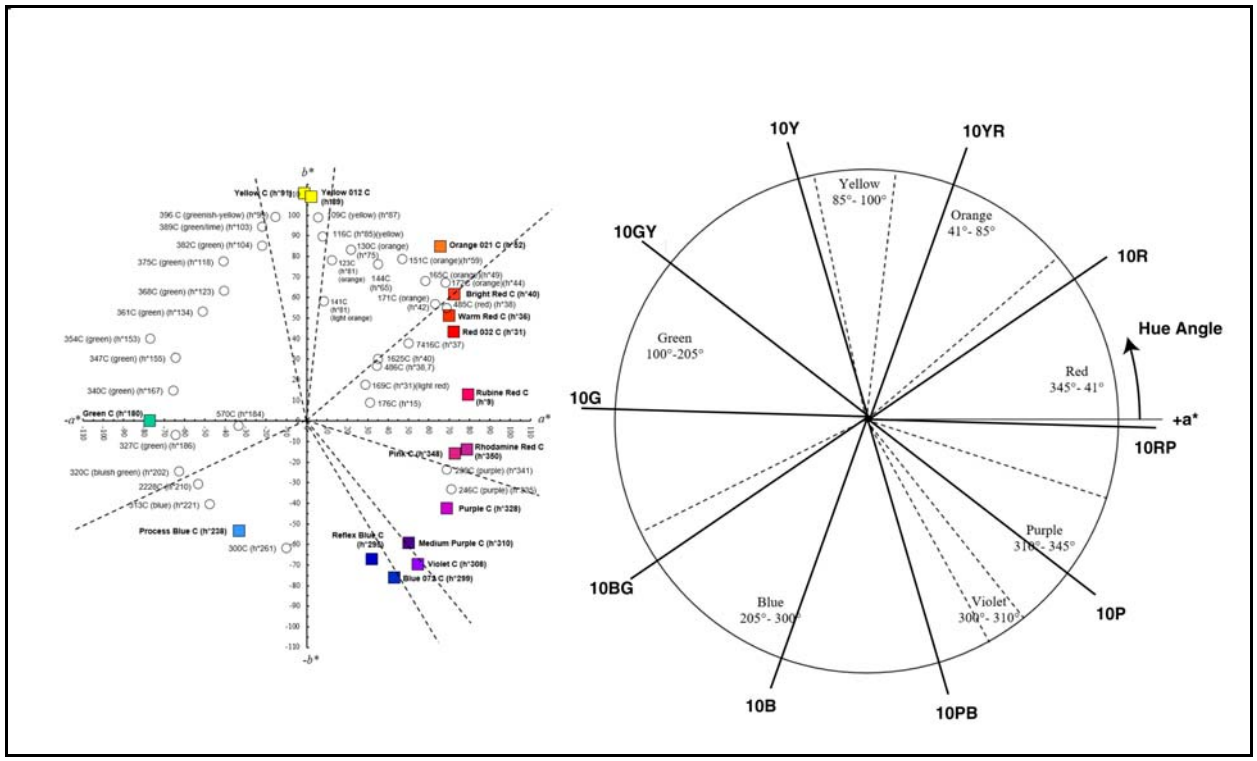


**Figure G.4.1-1 A collection of Pantone swatches plotted on a a*, b* color space. It is presented at this scale primarily for discussion. The radials shown on the right are from Munsell Color Space, rotated 16 degree ccw to better overlay the a*,b* space. xxx See text. From Abildgaard, 2019 (personal communications) with further annotation.**

The figure involves a series of questions to be considered.

Who developed this figure initially?
What is the name of the Pantone book used to obtain the color names?
Can it be assumed the color names are associated with spot colors (except where labeled process or reflex?
What does the term reflex refer to?
Was it obtained from one person or a group?
If a group, are the statistics associated with the different a*, b* values available?
What level of saturation is associated with the various circular locii in the figure?
Why are the a* and b* axes perpendicular when they are not on the CIE1931 Chromaticity Diagram?

## Table of Contents

Appendix G:
The Pantone “Our color Wheel” compared to the Chromaticity Diagram (2016) . . . . . 1
G.1 The Pantone color wheel versus the Chromaticity Diagram (2016) . . . . . 1
G.1.1 “Our Color Wheel” of Pantone . . . . . 1
G.1.2 The Chromaticity Diagram (2016) . . . . . 2
G.1.3 The archaic CIE representations up through 1975 . . . . . 4
G.1.3.1 The archaic chromaticity function as an example . . . . . 4
G.1.3.2 The archaic visibility function as an example . . . . . 4
G.1.4 Comparison of the Pantone color wheel and the Chromaticity Diagram (2016) . . . . . 7
G.2 The a*, b* color space . . . . . 9
G.2.1 The character of the a*, b* color space . . . . . 13
G.2.2 The a*, b* color space overlaid on the Chromaticity Diagram (2016 . . . . . 14
G.2.3 The a*, b* color space overlay in finer detail for small chroma (saturation) . . . . . 16
G.2.3.1 Corrections required to the CIELAB formulas . . . . . 17
G.2.3.1.1 Recommendation to correct rectilinearity at low chrominance values . . . . . 18
G.3 The definition of the pigments and lights optimally describing the human color space . . . . . 19
G.3.1 The character of the Chromaticity Diagram (2016) . . . . . 19
G.3.2 The spectra of ideal process color filters . . . . . 22
G.3.3 Review of the coloration of Abildgaard’s version of the CIEDE 2000 . . . . . 22
G.4 Defining Pantone color swatches within Color Spaces of the scientific community . . . . . 23

List of Figures

**Figure G.1.2-1** The Chromaticity Diagram (2016) . . . . . 3
**Figure G.1.3-1** Comparison of Visibility Functions . . . . . 5
**Figure G.1.3-2** Comparison of aphakic vision and the theoretical model . . . . . 6
**Figure G.1.4-1** "Our color wheel" from Pantone (top) compared to the Chromaticity Diagram (2016) . . . . . 8
**Figure G.2.1-1** The a*, b* Color Space associated with the CIEDE 2000 Standard . . . . . 10
**Figure G.2.1-2** Alternate coloration of the a*, b* color space ala Malarca . . . . . 11
**Figure G.2.1-3** The a*b* axes of CIELAB overlaid on the CIE x,y Chromaticity Diagram . . . . . 13
**Figure G.2.2-1** a*, b* axes overlaid on the Chromaticity Diagram (2016) . . . . . 15
**Figure G.2.3-1** A Munsell overlay at constant chroma onto a*, b* color space . . . . . 16
**Figure G.2.3-2** The center of the Chromaticity Diagram (2016) with a*, b* overlay . . . . . 17
**Figure G.3.1-1** Definition of the primary colors and their complement in human color space . . . . . 20
**Figure G.3.2-1** The ideal choice for the filters used in process color printing . . . . . 22
**Figure G.3.3-1** The a*, b* Color Space associated with the CIEDE 2000 Standard . . . . . 23
**Figure G.4.1-1** A collection of Pantone swatches plotted on a a*, b* color space . . . . . 24